Reconstruction of the three mechanical material constants of a lossy fluid-like cylinder from low-frequency scattered acoustic fields

Thierry Scotti, Armand Wirgin

Reconstruction of the three mechanical material constants of a lossy fluid-like cylinder from low-frequency scattered acoustic fields

Thierry Scotti* Armand Wirgin †

November 16, 2003

Abstract

The inverse medium problem for a circular cylindrical domain is studied using low-frequency acoustic waves as the probe radiation. It is shown that to second order in k_0a (k_0 the wavenumber in the host medium, a the radius of the cylinder), only the first three terms (i.e., of orders 0, -1 and +1) in the partial wave representation of the scattered field are non-vanishing, and the material parameters enter into these terms in explicit manner. Moreover, the zeroth-order term contains only two of the unknown material constants (i.e., the real and imaginary parts of complex compressibility of the cylinder κ_1) whereas the ± 1 order terms contain the other material constant (i.e., the density of the cylinder ρ_1). A method, relying on the knowledge of the totality of the far-zone scattered field and resulting in explicit expressions for ρ_1 and κ_1, is devised and shown to give highly-accurate estimates of these quantities even for frequencies such that k_0a is as large as 0.1.

Keywords: Inverse medium problem; acoustics

*Laboratoire de Mécanique et d'Acoustique, UPR 7051 du CNRS, 31 chemin Joseph Aiguier, 13009 Marseille, France, wirgin@lma.cnrs-mrs.fr

†Laboratoire de Mécanique et d'Acoustique, UPR 7051 du CNRS, 31 chemin Joseph Aiguier, 13009 Marseille, France, ogam@lma.cnrs-mrs.fr

1 Introduction

Retrieving the mechanical material constants (e.g., elastic moduli, density) of a material, either by direct measurements of these quantities, or by measurements of other variables from which the material constants can be derived with the help of suitable models, is one of the central problems in materials science. When the specimen is a solid, the elastic moduli are determined either by the usual static methods or by dynamic methods involving the inversion of data relative to resonant frequencies and/or mode shapes of vibrations excited, for instance by percussive forces [5], [20], [10], [16], or relative to velocities and attenuations for ultrasonic wave probe radiation [13]. Ultrasound methods can also be employed for fluids, or fluid-like materials [13], [17].

Another class of material characterization methods, called *resonance spectroscopy* [2] combines the underlying principles of vibratory resonances with an acoustic excitation of the specimen. This technique has also been employed to determine the refractive index of beads by means of laser irradiation [6]. This class of techniques differs from the previous ones in that it relies on measurements of the *wavefield diffracted by the specimen*, and appeals to a quite intricate theory relating the resonances to coefficients computed from the diffracted field for estimating the material parameters (it can also be employed for estimating the geometrical parameters of the specimen [6], [2], [7]). This theory is only feasible for specimens having simple geometry (e.g., spherical, circular cylindrical, plate-like). A simple specimen geometry is also required in the standard vibration-resonance and velocity-attenuation methods if absolute quantitative characterizations are aimed at.

During the last 25 years, another materials-characterization method has been developed which can be termed *wavefield imaging*. The underlying idea is: i) acquire measurements of the field scattered from a specimen at a series of locations in space arising either from several monochromatic probe fields, and/or from a pulse-like probe field, and ii) retrieve from these measurements an *image* of the specimen (i.e., a spatial map of some material characteristic, such as wavespeed or attenuation) with the help of a suitable model of the specimen/wave interaction. Insofar as there is a sharp difference between the material properties of the specimen and those of the host medium, this method also gives a picture of the geometry (location, orientation, size and shape) of the specimen. When, as is often the case, the information relating to the material constants of the specimen is not reliable, only the geometrical information can been exploited (this is called *qualitative wavefield imaging*; otherwise it is called *quantitative wavefield imaging*). For instance, computerized diffraction tomography, making use of a model appealing either to the Rytov or Born approximations of the specimen/wave interaction, is a qualitative wavefield imaging technique except for specimens whose properties differ only slightly from those of the host medium (this is fortunately the case in biological imaging applications) [17], [19], [9], [8]. It has been suggested [19], [9], [8] that one of the reasons why Born-based techniques do not furnish reliable estimates of the material properties (notably the wavespeed, in specimens assumed to be lossless and surrounded by a host medium which is also lossless and has the same density as that of the specimen), is that data relating to low-frequency probe radiation was either not available or not used in the inversion algorithm.

The importance of disposing of multi-frequency (and, in particular, low frequency) data is increasingly recognized as the key to success for material characterization in wavefield

imaging techniques such as the distorted Born method [11], [18], the modified Born and modified gradient methods [3], and the contrast source method [4]. The possibility of obtaining a quantitatively-accurate image with these iterative methods is often dependent on being able to initialize the algorithm with a plausible image of the object at the lowest frequency of the probe radiation. More often than not, this initial image is obtained via the Born approximation, and since the latter is not accurate for large contrasts (between the host and the object) of the material constants, the algorithm has trouble with restoring the right values of the material constants during the iterative process. Thus, it would be useful to find a means for obtaining a better estimate of the material constants at low frequencies in the case of arbitrarily-large contrasts. This is done herein.

In particular, we shall be concerned with the retrieval of the three material constants $\Re\kappa_1$, $\Im\kappa_1$ and ρ_1 (wherein $\kappa_1 = \Re\kappa_1 + i\Im\kappa_1$) of a generally-lossy fluid object in a lossless fluid host probed by plane-wave acoustic radiation. The case $\Im\kappa_1 = 0$ of a lossless material can also be treated. No assumption is made concerning the contrasts of density and compressibility between the host and the object. The latter is assumed to be a circular cylinder, of known radius a. The material constants of the host medium (in which the probe radiation propagates) are also assumed to be known, as is known the frequency and incident angle of the plane wave probe radiation, as well as the scattered acoustic wavefield in the far zone of the cylinder. The analysis for recovering the three material parameters of the cylinder is focused on the case in which the wavelength ($\lambda_0 = 2\pi/k_0$, with $k_0 = \omega/c_0$, c_0 the speed of bulk waves in the host, and ω the angular frequency) of the probe radiation is much larger than the cylinder radius.

2 Physical configuration and governing equations

The scattering body is an infinite cylinder whose generators are parallel to the z axis in the cylindrical polar coordinate system (r, θ, z). The intersection of the cylinder, within which is located the origin O, with the xOy plane defines (see figure 1):

i) the boundary curve $\Gamma = \{r = \rho(\theta); 0 \leq \theta < 2\pi\}$, with ρ a continuous, single-valued function of θ (further on, we shall take Γ to be a circle, i.e., $\rho(\theta) = a$),

ii) the bounded (inner) region (i.e., that occupied by the body in its cross-section plane) $\Omega_1 = \{r < \rho(\theta); 0 \leq \theta < 2\pi\}$,

iii) the unbounded (outer) region $\Omega_0 = \{r > \rho(\theta); 0 \leq \theta < 2\pi\}$.

It is assumed that Ω_0 and Ω_1 are filled with linear, homogeneous, isotropic, time-invariant fluid-like media M_0 and M_1 respectively and that M_1 is possibly lossy.

The cylinder is probed by a monochromatic acoustic plane whose propagation vector lies in the xOy plane. Due to the invariance of the cylinder and incident field with respect to z, the incident and scattered field is also invariant with respect to z. Let U designate pressure, which, due to the previously-mentioned invariance, is of the form:

$$U = U(\mathbf{x}, t) \ , \tag{1}$$

with $\mathbf{x} = (x, y) = (r, \theta)$. This invariance applies also when superscripts i and d (i for 'incident' and d for 'diffracted') are attached to U. It is convenient to associate $U(\mathbf{x}, t)$ with

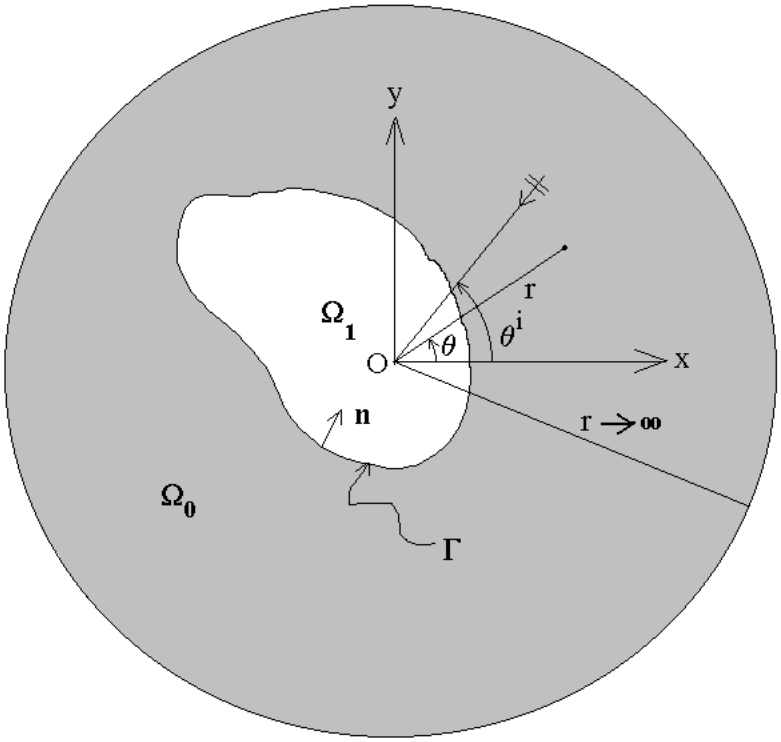

Figure 1: Problem configuration in the xOy plane

the total field, it being understood that the latter takes the form $U_j(\mathbf{x}, t)$ in Ω_j and:

$$U_j(\mathbf{x}, t) = U^i(\mathbf{x}, t)\delta_{j0} + U_j^d(\mathbf{x}, t) \ ; \ \mathbf{x} \in \Omega_j \ , \tag{2}$$

with δ_{jk} the Kronecker delta.

We express U by the Fourier transform

$$U_j(\mathbf{x}, t) = \int_{-\infty}^{\infty} u_j(\mathbf{x}, \omega) \exp(-i\omega t) d\omega \ , \tag{3}$$

with similar expressions for U^i and U^d. The monochromatic, plane-wave nature of the incident field is such that

$$u^i(\mathbf{x}, \omega) = \exp\left[-ik_0 r \cos\left(\theta - \theta^i\right)\right] \ , \tag{4}$$

wherein θ^i designates the incident angle.

The essential task in both the forward and inverse scattering contexts is to determine

$$u_j(\mathbf{x}, \omega) = u^i(\mathbf{x}, \omega)\delta_{j0} + u_j^d(\mathbf{x}, \omega) \ ; \ \mathbf{x} \in \Omega_j \ . \tag{5}$$

via the governing equations:

$$(\Delta + k_j^2) u_j(\mathbf{x}, \omega) = 0 \ ; \ \mathbf{x} \in \Omega_j \quad , \quad j = 0, 1 \ , \tag{6}$$

$$\lim_{r\to\infty} r^{1/2}(\partial_r - ik_0)u_0^d(\mathbf{x},\omega) = 0 \ ; \ \forall\theta \in [0, 2\pi[\ , \tag{7}$$

$$|u_1^d(\mathbf{x},\omega)| < \infty \ ; \ \mathbf{x} \in \Omega_1 \ , \tag{8}$$

$$u_0(\mathbf{x},\omega) - u_1(r,\theta,\omega) = 0 \ ; \ \mathbf{x} \in \Gamma \ , \tag{9}$$

$$\alpha_0 \mathbf{n}\cdot\nabla u_0(\mathbf{x},\omega) - \alpha_1 \mathbf{n}\cdot\nabla u_1(\mathbf{x},\omega) = 0 \ ; \ \mathbf{x} \in \Gamma \ , \tag{10}$$

wherein $\mathbf{n}$ is the unit vector normal to Γ and:

$$k_j^2 = \omega^2 (c_j)^{-2} \ , \quad c_j^2 = (\rho_j \kappa_j)^{-1} \ , \quad \alpha_j = (\rho_j)^{-1} \ . \tag{11}$$

3 Forward and inverse scattering problems

The *forward scattering problem* (notably for simulating measured data) is formulated as follows:
given:

i) the location, shape, size and composition (material properties) of the scattering body,

ii) the material properties of the host medium M_0

iii) the incident wavefield (i.e., (4), as well as the frequency thereof,

determine:

the field (i.e., $u_j^d \ ; \ j = 0, 1$) scattered by the body at arbitrary points of space.

The general *inverse scattering problem* is formulated as follows:
given:

i) the incident wavefield (i.e., (4)), as well as the frequency thereof,

ii) the material properties of the host medium M_0

ii) the wavefield in some subregion of Ω_0,

reconstruct:

the location, shape, size and composition of the scattering body.

Hereafter, we shall be concerned mostly with the *inverse problem*, and, in particular, with one in which the location, size and shape of the body are known beforehand, the task being to reconstruct the *composition* of the body.

In fact, the body will be chosen to be a *homogeneous cylinder with center at the origin* O and radius a, and we will try to reconstruct its material properties ρ_1 and κ_1 from the scattered acoustic field for *low-frequency probe radiation.*

4 Partial wave expressions of the fields

A well-known identity [1] informs us that the plane-wave probe radiation admits the partial wave expansion

$$u^i(\mathbf{x},\omega) = \sum_{m=-\infty}^{\infty} \gamma_m J_m(k_0 r) \exp\left(im\theta\right) \ ; \ \forall \mathbf{x} \in \mathbb{R}^2 \ . \tag{12}$$

wherein $J_m(\ \ )$ is the m-th order Bessel function and

$$\gamma_m = \exp\ (-im(\theta^i + \pi/2)\ )\ . \tag{13}$$

By applying the separation of variables technique to (6) and (7), it is found that

$$u_0^d(\mathbf{x},\omega) = \sum_{m=-\infty}^{\infty} C_m H_m^{(1)}(k_0 r) \exp\ (im\theta\ )\ \ ;\ \ \forall \mathbf{x} \in \Omega_0\ , \tag{14}$$

wherein $H_m^{(1)}(\ \ )$ is the m-th order Hankel function. The application of the same technique to (6) and (8) gives

$$u_1^d(\mathbf{x},\omega) = \sum_{m=-\infty}^{\infty} D_m J_m(k_1 r) \exp\ (im\theta\ )\ \ ;\ \ \forall \mathbf{x} \in \Omega_1\ . \tag{15}$$

From the transmission conditions (9) and (10) we deduce, due to the orthogonality of the functions $\{\exp(im\theta)\}$, the fact that $\rho(\theta) = a$ and $\mathbf{n}\cdot\nabla = -\partial_r$ in the present case,

$$C_m = \gamma_m \frac{J_m(k_0a)\dot{J}_m(k_1a) - \beta \dot{J}_m(k_0a) J_m(k_1a)}{\beta \dot{H}_m^{(1)}(k_0a) J_m(k_1a) - H_m^{(1)}(k_0a)\dot{J}_m(k_1a)}\ , \tag{16}$$

$$D_m = \gamma_m \beta \frac{J_m(k_0a)\dot{H}_m^{(1)}(k_0a) - \dot{J}_m(k_0a) H_m^{(1)}(k_0a)}{\beta \dot{H}_m^{(1)}(k_0a) J_m(k_1a) - H_m^{(1)}(k_0a)\dot{J}_m(k_1a)}\ , \tag{17}$$

wherein: $Z_m(\xi) = J_m(\xi)$, $Z_m(\xi) = Y_m(\xi)$ or any linear combination thereof, knowing that $H_m^{(1)}(\xi) = J_m(\xi) + iY_m(\xi)$, with $Y_m(\xi)$ the m-th order Neumann function), $\dot{Z}(\xi) := dZ(\xi)/d\xi$ and $\beta = k_0\alpha_0/k_1\alpha_1$.

5 Low-frequency approximation of the scattered field outside of the body and inversion formulas

We use the formulas [1]

$$\dot{Z}_m(\xi) = Z_{m-1}(\xi) - \frac{m}{\xi} \dot{Z}_m(\xi)\ ,\quad Z_{-m}(\xi) = (-1)^m Z_m(\xi)\ , \tag{18}$$

to find:

$$\dot{Z}_0(\xi) = -Z_1(\xi)\ , \tag{19}$$

and

$$C_0 = \gamma_0 \frac{-J_0(k_0a)J_1(k_1a) + \beta J_1(k_0a) J_0(k_1a)}{-\beta H_1^{(1)}(k_0a) J_0(k_1a) + H_0^{(1)}(k_0a) J_1(k_1a)}\ , \tag{20}$$

$$C_{\pm 1} = \gamma_1 \frac{J_1(k_0a)\left[J_0(k_1a) - (k_1a)^{-1}J_1(k_1a)\right] - \beta J_1(k_1a)\left[J_0(k_0a) - (k_0a)^{-1}J_1(k_0a)\right]}{\beta J_1(k_1a)\left[H_0^{(1)}(k_0a) - (k_0a)^{-1}H_1^{(1)}(k_0a)\right] - H_1^{(1)}(k_0a)\left[J_0(k_1a) - (k_1a)^{-1}J_1(k_0a)\right]}\ , \tag{21}$$

etc.

We employ the notation:

$$\zeta := k_1/k_0 \ , \quad \delta := k_0 a \ . \tag{22}$$

Due to the hypothesis of low frequencies (and/or small cylinder radius),

$$\delta << 1 \ . \tag{23}$$

We employ the small-argument asymptotic forms of the Bessel and Neumann functions [1]

$$J_0(\delta) \sim 1 - \delta^2/4 \ \ , \ \ J_1(\delta) \sim \delta/2 \ \ , \ \ Y_0(\delta) \sim (2/\pi)\ln\delta \ \ , \ \ Y_1(\delta) \sim -2/\pi\delta \ \ ; \ \ \delta \to 0 \ , \tag{24}$$

to find

$$C_0 \sim \tilde{C}_0 := -\gamma_0 \frac{i\pi\delta^2}{4\beta}(-\zeta + \beta) \ \ ; \ \ \delta \to 0 \ , \tag{25}$$

$$C_{\pm 1} \sim \tilde{C}_{\pm 1} := -\gamma_1 \frac{i\pi\delta^2}{4} \frac{1-\zeta\beta}{1+\zeta\beta} \ \ ; \ \ \delta \to 0 \ . \tag{26}$$

Thus, C_0 and $C_{\pm 1}$ are $\mathcal{O}(\delta^2)$ as $\delta \to 0$. In the same way we show that $C_{|m|>1}$ vanishes faster than δ^2, so that to second order in δ we can write

$$u_0^d(\mathbf{x},\omega) \sim \sum_{m=-1}^{1} \tilde{C}_m H_m^{(1)}(k_0 r) \exp\ (im\theta\ ) \ \ ; \ \ \forall \mathbf{x} \in \Omega_0 \ \ ; \ \ \delta \to 0 \ , \tag{27}$$

or, in other terms,

$$u_0^d(\mathbf{x},\omega) \sim \frac{i\pi\delta^2}{4}\frac{\zeta-\beta}{\beta} H_0^{(1)}(k_0 r) - \frac{\pi\delta^2}{2}\frac{1-\zeta\beta}{1+\zeta\beta} H_1^{(1)}(k_0 r)\cos(\theta - \theta^i) \ \ ; \ \ \forall \mathbf{x} \in \Omega_0 \ \ ; \ \ \delta \to 0 \ . \tag{28}$$

It is customary, but not necessary, to measure the field in the far-field zone. In this case, we employ the large-argument asymptotic form of the Hankel functions [1]:

$$H_n^{(1)}(\xi) \sim \sqrt{\frac{2}{\pi\xi}} \exp\left[i\left(\xi - \frac{n\pi}{2} - \frac{\pi}{4} \right) \right] \ \ ; \ \ \xi \to \infty \ , \tag{29}$$

to find:

$$u_0^d(\mathbf{x},\omega) \sim \breve{u}_0^d(\theta,\theta^i,\omega) \sqrt{\frac{2}{\pi k_0 r}} \exp\left[i\left(k_0 r - \frac{\pi}{4} \right) \right] \ \ ; \ \ k_0 r \to \infty \ , \tag{30}$$

wherein, the so-called *far-field scattering function* is given (in the asymptotic low-frequency regime) by

$$\breve{u}_0^d(\theta,\theta^i,\omega) \sim \frac{i\pi\delta^2}{4}\left[\frac{\zeta-\beta}{\beta} - 2\left(\frac{\zeta\beta - 1}{\zeta\beta + 1} \right) \cos(\theta - \theta^i) \right] \ \ ; \ \ \delta \to 0 \ . \tag{31}$$

Using (11) we find that (28) and (31) become:

$$u_0^d(\mathbf{x},\omega) \sim \frac{i\pi(k_0 a)^2}{4}\left[\left(\frac{\kappa_1}{\kappa_0} - 1 \right) H_0^{(1)}(k_0 r) - 2i \left(\frac{\frac{\rho_1}{\rho_0} - 1}{\frac{\rho_1}{\rho_0} + 1} \right) H_1^{(1)}(k_0 r)\cos(\theta - \theta^i) \right]$$
$$; \ \ \forall \mathbf{x} \in \Omega_0 \ \ ; \ \ (k_0 a) \to 0 \ , \tag{32}$$

$$\breve{u}_0^d(\theta,\theta^i,\omega) \sim \frac{i\pi(k_0a)^2}{4}\left[\left(\frac{\kappa_1}{\kappa_0}-1\right)-2\left(\frac{\frac{\rho_1}{\rho_0}-1}{\frac{\rho_1}{\rho_0}+1}\right)\cos(\theta-\theta^i)\right] \;\;;\;\; \delta\to 0\ . \tag{33}$$

The general problem in (32) and (33) is to express A and B in terms of $C(\theta)$; $\forall\theta\in[0,2\pi[$ knowing that

$$C(\theta)=A+B\cos(\theta-\theta^i) \;\;;\;\; \forall\theta\in[0,2\pi[\ . \tag{34}$$

Then

$$\int_0^{2\pi} C(\theta)\cos n\theta d\theta = A\int_0^{2\pi}\cos n\theta d\theta + B\int_0^{2\pi}\cos(\theta-\theta^i)\cos n\theta d\theta \;\;;\;\; \forall n\in\mathbb{Z}\ . \tag{35}$$

from which we find:

$$A=\frac{1}{2\pi}\int_0^{2\pi}C(\theta)d\theta \;\;,\;\; B=\frac{1}{\pi\cos\theta^i}\int_0^{2\pi}C(\theta)\cos\theta d\theta\ . \tag{36}$$

Applied to (33), this gives:

$$\kappa_1=\kappa_0\left[1+\frac{4}{i\pi(k_0a)^2}\frac{1}{2\pi}\int_0^{2\pi}\breve{u}_0^d(\theta,\theta^i,\omega)d\theta\right]\ , \tag{37}$$

$$\rho_1=\rho_0\left[\frac{1-\frac{2}{i\pi(k_0a)^2}\frac{1}{\pi\cos\theta^i}\int_0^{2\pi}\breve{u}_0^d(\theta,\theta^i,\omega)\cos\theta d\theta}{1+\frac{2}{i\pi(k_0a)^2}\frac{1}{\pi\cos\theta^i}\int_0^{2\pi}\breve{u}_0^d(\theta,\theta^i,\omega)\cos\theta d\theta}\right]\ . \tag{38}$$

This shows that: i) κ_1 can be retrieved independently of ρ_1, ii) κ_1 is a linear function of the measured scattered field, whereas iii) ρ_1 is a nonlinear function of this field. More importantly: (37)-(38) constitute a method for determining ρ_1 and the real and imaginary parts of κ_1 from the (far-field) scattering function, in an explicit, analytic manner.

6 Numerical results

We applied formulas (37) and (38) to retrieve the density and complex compressibility from the far-field scattering function. More precisely, we computed the relative errors (see figures 2-4):

$$\delta_{\rho_1}:=\left|\frac{\tilde{\rho_1}-\rho_1}{\rho_1}\right|,\;\; \delta_{\Re\kappa_1}:=\left|\frac{\Re\tilde{\kappa}_1-\Re\kappa_1}{\Re\kappa_1}\right|,\;\; \delta_{\Im\kappa_1}:=\left|\frac{\Im\tilde{\kappa}_1-\Im\kappa_1}{\Im\kappa_1}\right|, \tag{39}$$

(wherein $\tilde{\rho}_1$ is the value of density obtained from (38), and $\Re\tilde{\kappa}_1$, $\Im\tilde{\kappa}_1$ the values of the real and imaginary parts of the complex compressibility obtained from (37)) over a range of frequencies corresponding to $10^{-5}\leq k_0a\leq 1.5$. The far-field data was simulated using (14) in which the lower and upper limits of the series were replaced by -5 and +5 respectively and use was also made of (30). The other parameters involved in the production of this data were: $\rho_0=1000\ kg/m^3$, $c_0=1500\ m/s$, $\rho_1=1200\ kg/m^3$, $c_1=2500+i250\ m/s$, $\theta^i=0$, $a=1.0\ m$. One sees from figures 2-4 that in order to get relative errors of the mechanical material parameters inferior or equal to 5%, the probe frequency should be such that k_0a is not greater than ~ 0.1.

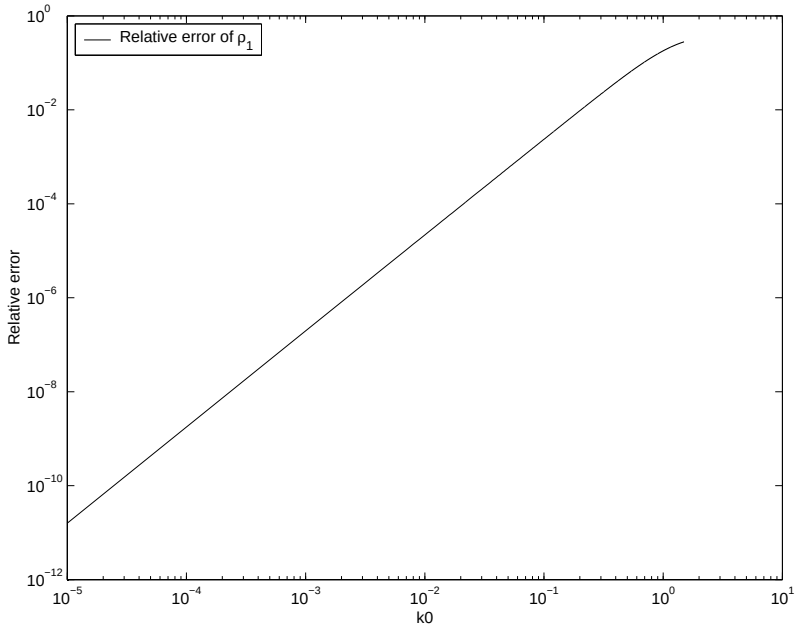

Figure 2: Relative error of ρ_1

7 Conclusion

Low frequency probe radiation is interesting in that it provides solutions to the inverse medium problem which can be written in *closed form* and which are *unique*. Moreover, these solutions do not rely (as those appealing to the Born approximation) on any assumptions concerning the compressibility and density contrasts. Thus, the results presented herein are valid for arbitrary values of these contrasts.

At the worst, the solutions of the inverse problem treated with low-frequency probe radiation provide suitable starting solutions for reconstructions carried out with higher-frequency probe radiation as well as possible explanations of the difficulties encountered in inverse medium problems such as the one considered herein. They may also provide decent estimates of the material parameters of homogeneous (and even inhomogeneous) bodies of more general shapes.

In case the characteristic dimension of the body (here the radius a) is not known a priori, it can be determined from high-frequency probe radiation using the asymptotic technique described in [12], [14] [15].

The method outlined herein is obviously transposable to: homogeneous fluid slabs and spheres, homogeneous elastic slabs, circular cylinders and spheres, and to fluid-like or elastic circular tubes and spherical shells.

References

[1] M. Abramowitz, A. Stegun, Handbook of Mathematical Functions, Dover, New York, 1968.

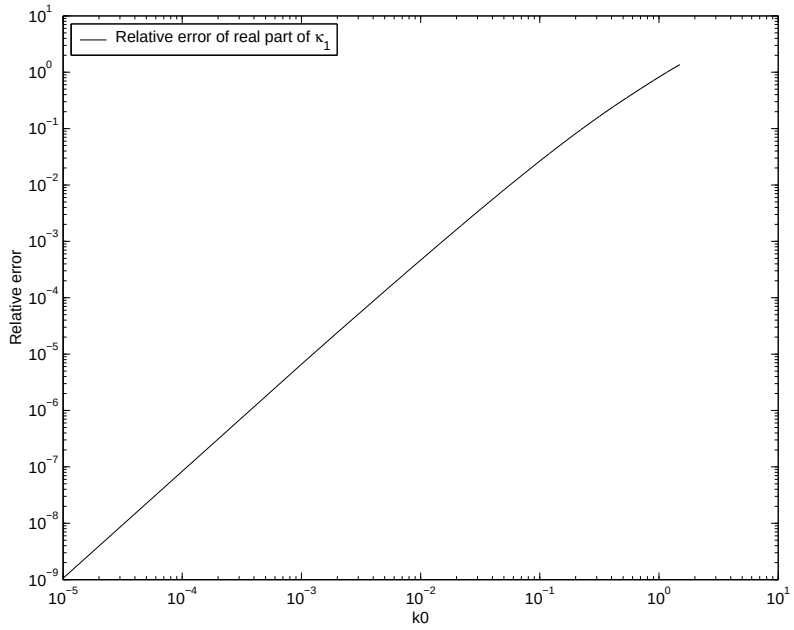

Figure 3: Relative error of $\Re\kappa_1$

[2] J.D. Alemar, P.P. Delsanto, E. Rosario, Spectral analysis of the scattering of acoustic waves from a fluid cylinder. III. Solution of the inverse scattering problem, Acustica, 61 (1986) 14-20.

[3] K. Belkebir and A.G. Tijhuis, Modified gradient method and modified Born method for solving a two-dimensional inverse scattering problem, Inverse Probs., 17 (2001) 1671-1688.

[4] R.F. Bloemenkamp, A. Abubakar, P.M. van de Berg, Inversion of experimental multi-frequency data using the contrast source inversion method, Inverse Probs., 17 (2001) 1611-1622.

[5] P. Cawley and R.D. Adams, Vibration Techniques, in: Non-Destructive Testing of Fibre-Reinforced Plastics Composites, Vol. 1, J. Summerscales (ed.), Elsevier, London, 1987, pp.151-205.

[6] P. Chylek, V. Ramaswamy, A. Ashkin, J.M. Dziedzic, Simultaneous determination of refractive index and size of spherical dielectric particles from light scattering data, Appl.Opt., 22 (1983) 2302-2307.

[7] A.K. Datta, S.C. Som, On the inverse scattering problem for dielectric cylindrical scatterers, IEEE Trans. Anten.Prop. 29 (1981) 392-397.

[8] S. Delamare, Sur l'approximation de Born dans la tomographie ultrasonore, Doctoral thesis, Université Aix-Marseille II, Marseille, 1999, pp. 62-64.

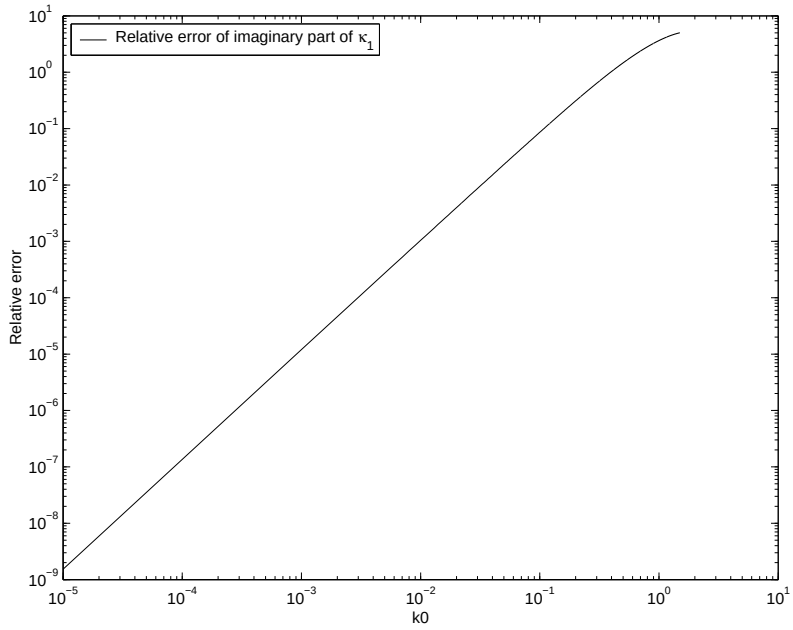

Figure 4: Relative error of $\Im\kappa_1$

[9] S. Delamare, J.-P. Lefebvre, P. Lasaygues, Back scattered ultrasonic tomography: experiments and modelizations, in: Acoustical Imaging, Vol.23, S. Lees, L.A. Ferrari (eds.), Plenum Press, New York, 1997, pp. 595-600.

[10] J.E. Grady, B.A. Lerch, Effect of heat treatment on stiffness and damping of SIC/Ti-15-3, in: Vibro-Acoustic Characterization of Materials and Structures, NCA-Vol.14, P.K. Raju (ed.), ASME, New York, 1992, pp. 13-20.

[11] O.S. Haddadin, E.S. Ebbini, Multiple frequency distorted Born iterative method for tomographic imaging, in: Acoustical Imaging, Vol.23, S. Lees, L.A. Ferrari (eds.), Plenum Press, New York, 1997, pp. 613-619.

[12] J.R. Hodkinson, Particle sizing by means of the forward scattering lobe, Appl.Opt. 5 (1966) 839-844.

[13] J. Krautkramer, H. Krautkramer, Ultrasonic Testing of Materials, Springer, New York, 1969.

[14] D. Lebrun, S. Belaid, C. Ozkul, K.F. Ren, G. Gréhan, Enhancement of wire diameter measurements: comparison between Fraunhofer diffraction and Lorenz-Mie theory, Opt.Engrg. 35 (1996) 946-950.

[15] P.M. Morse P.M. and H. Feshbach, Methods of Theoretical Physics, McGraw-Hill, New York, 1953, p. 1381, 1554.

[16] M.F. Nelson, J.A. Wolf Jr., A nondestructive technique for determining the elastic constants of advanced composites, in: Vibro-Acoustic Characterization of Materials and Structures, NCA-Vol.14, P.K. Raju (ed.), ASME, New York, 1992, pp. 227-233.

[17] B.S. Robinson, J.F. Greenleaf, The scattering of ultrasound by cylinders: implications for diffraction tomography, J.Acoust.Soc.Am., 80 (1986) 40-49.

[18] A.G. Tijhuis, K. Belkebir, A.C.S. Litman, B. P. de Hon, Multiple-frequency distorted-wave Born approach to 2D inverse profiling, Inverse Probs., 17 (2001) 1635-1644.

[19] W. Tobocman, In vivo biomicroscopy with ultrasound, Current Topics in Acoust.Res., 1 (1994) 247-265.

[20] A. Vary, Acousto-ultrasonics, in: Non-Destructive Testing of Fibre-Reinforced Plastics Composites, Vol. 2, J. Summerscales (ed.), Elsevier, London, 1990, pp. 1-54.